

## Review

# Noninvasive imaging of the PD-1:PD-L1 immune checkpoint: Embracing nuclear medicine for the benefit of personalized immunotherapy

Katrijn Broos<sup>1</sup>, Quentin Lecocq<sup>1</sup>, Geert Raes<sup>2,3</sup>, Nick Devoogdt<sup>4</sup>, Marleen Keyaerts<sup>4,5</sup>✉, Karine Breckpot<sup>1</sup>✉

1. Laboratory of Molecular and Cellular Therapy (LMCT), Vrije Universiteit Brussel (VUB), Laarbeeklaan 103, B-1090 Brussels
2. Unit of Cellular and Molecular Immunology (CMIM), VUB, Pleinlaan 2, B-1050 Brussels
3. Myeloid Cell Immunology Lab, VIB Inflammation Research Center, Pleinlaan 2, B-1050 Brussels, Belgium
4. *In Vivo* Cellular and Molecular Imaging Laboratory (ICMI), VUB, Laarbeeklaan 103, B-1090 Brussels
5. Nuclear Medicine Department, UZ Brussel, Laarbeeklaan 101, B-1090 Brussels

✉ Corresponding authors: Karine Breckpot: Tel: 0032-2-477.45.65, Mail: karine.breckpot@vub.be. Marleen Keyaerts: Tel: 0032-2-477.50.20, Mail: marleen.keyaerts@vub.ac.be.

© Ivyspring International Publisher. This is an open access article distributed under the terms of the Creative Commons Attribution (CC BY-NC) license (<https://creativecommons.org/licenses/by-nc/4.0/>). See <http://ivyspring.com/terms> for full terms and conditions.

Received: 2018.01.05; Accepted: 2018.03.23; Published: 2018.06.07

## Abstract

Molecular imaging of the immune checkpoint receptor PD-1 and its ligand PD-L1 is increasingly investigated as a strategy to guide and monitor PD-1:PD-L1-targeted immune checkpoint therapy. We provide an overview of the current state-of-the-art on PD-1- and PD-L1-specific imaging agents for quantitative, real-time assessment of PD-1:PD-L1 expression in the tumor environment and discuss their potential for clinical translation.

Key words: PD-1:PD-L1, biomarker, molecular imaging, immunotherapy

## Introduction

### PD-1:PD-L1 immune checkpoint therapy

The concept of manipulating the immune system to induce clinically relevant responses against cancer is longstanding. Interventions to enhance tumor-specific immunity like vaccination and adoptive T cell transfer have resulted in clinical successes in individual cases [1]. However, cancer immunotherapy did not mature to take its place as oncology's vanguard until the advent of immune checkpoint inhibition and the major improvement in survival it heralded [2,3].

The immune checkpoint with the widest clinical applications is that composed of the programmed cell death-1 (PD-1, CD279) receptor and its ligand programmed cell death-ligand 1 (PD-L1, CD274, B7-H1). The rising interest in this inhibitory immune checkpoint stems from the knowledge that PD-L1 is expressed intrinsically on a variety of tumor cells, while other tumor cells upregulate PD-L1 expression

in response to inflammatory cytokines, a phenomenon known as adaptive resistance [4,5].

Furthermore, PD-L1 is expressed on tumor-associated myeloid cells such as dendritic cells that intimately interact with CD8<sup>pos</sup> tumor-infiltrating T cells [6]. CD8<sup>pos</sup> immune effector cells express high levels of PD-1, an inhibitory receptor that upon binding to PD-L1 induces anergy and even cell death [7]. Monoclonal antibodies (mAbs) that bind PD-1 or PD-L1, thereby blocking their interaction, have been shown to enhance anticancer immunity in many preclinical studies. More importantly, clinical trials with anti-PD-1 and anti-PD-L1 mAbs have shown unprecedented results in cancer patients that are already heavily treated with and became refractory to other conventional therapy options [8-15]. As a consequence, the FDA accelerated the approval of anti-PD-1 mAbs pembrolizumab and nivolumab, and anti-PD-L1 mAbs durvalumab, atezolizumab and avelumab, which have since become available as

standard-of-care for several cancer types. The downside of this success story is the high cost of such treatments, easily surpassing \$100,000 per patient [16], and the observation that these immune checkpoint blockers are only of benefit for a subset of patients [17]. The failure rate, combined with the high cost for society, drives the search for predictive biomarkers that can help select the right treatment for the right patient.

<sup>18</sup>F-fluorodeoxyglucose (FDG) PET/CT is routinely used in cancer patients for staging and disease monitoring. Recent reports have highlighted its potential to assess treatment responses to immune checkpoint inhibition therapy at earlier time points than anatomical imaging [18–21]. Its importance in predicting outcome prior to treatment remains to be determined, but is expected to be much lower, leaving an opportunity for other imaging procedures, such as PD-1 or PD-L1 expression imaging.

### PD-1 and PD-L1 expression levels as predictive biomarkers

The PD-1:PD-L1 interaction is known to occur in the tumor microenvironment, where immune cells that express PD-1 are inactivated by expression of PD-L1 on tumor cells and a number of tumor-infiltrating immune cells. In patients with various types of advanced solid cancer, the PD-L1 status of the tumor, using immunohistochemical staining (IHC), was correlated to the outcome of PD-1:PD-L1 blockade, and it was observed that responses were significantly higher in PD-L1-expressing tumors: 9 of 25 patients with PD-L1-expressing (PD-L1<sup>pos</sup>) tumors responded, while none of 17 patients with PD-L1-nonexpressing (PD-L1<sup>neg</sup>) tumors responded [22]. However, in subsequent studies, responses were also observed in PD-L1<sup>neg</sup> cancers, although to a much lesser extent. This could be due to the effect of PD-1:PD-L1 blockade occurring outside of the tumor microenvironment due to heterogeneity of PD-L1 expression in cancer lesions, which is not always correctly assessed by core needle biopsy, or due to changes in PD-L1 expression over time, which is in current trials sometimes assessed using repeated biopsies. Within the patient group with expression of PD-L1 in a tumor biopsy, the majority of patients do not respond to the blockade treatment, indicating that the expression of PD-L1 on its own is not always sufficient for treatment response prediction, likely because of a lack of immune activation—potentially linked to a low tumor mutational burden—or because of resistance mechanisms, e.g., the role of PD-L1 expression on host cells [23,24]. Further complicating matters, different companies have developed distinct companion assays for PD-L1

expression, each using different IHC antibodies, interpretations (expression on tumor cells, immune cells or both) and thresholds for positivity. Therefore, in the Blueprint project, 39 NSCLC tumors were evaluated for PD-L1 positivity using four different PD-L1 IHC assays, 22C3, 28-8, SP263 and SP142. 22C3 pharmDx and 28-8 pharmDx are already FDA-approved and used in clinical routine for the selection of lung cancer patients. The study revealed that three of the four IHC assays, 22C3, 28-8 and SP263, were able to similarly detect PD-L1 expression on tumor cells, whereas SP142 showed less stained tumor cells. On the other hand, staining for PD-L1 on immune cells revealed higher variety between the four staining assays. Moreover, using all four assays, 50% of the tested patients would be classified above the selected cut-off and 13% below the selected cut-off. The other 37% varied in classification above or below assay-associated cut-offs, likely due to a variation in cut-off definition, confirming the shortcomings of IHC [25,26]. Overall, it was shown across 15 studies of solid tumors that the response rate for PD-L1<sup>pos</sup> tumors was 48%, compared to 15% amongst PD-L1<sup>neg</sup> tumors [27]. Although much less convincing, some data are available for a correlation between PD-1 expression on tumor-infiltrating T cells and treatment outcome [28].

In summary, currently the most commonly used predictive biomarker is PD-L1 expression assessed via IHC on tumor biopsies, although limitations are obviously present. Limitations such as heterogeneous expression, the role of expression outside of the tumor, and its dynamic expression during the disease process could be overcome by noninvasive molecular imaging using radiolabeled tracers that allow deep tumor penetration and repeated quantification of PD-1 and/or PD-L1 expression, which should enable mapping of primary tumors and metastatic lesions both before and during the treatment. Its potential as a tool to provide an accurate assessment of PD-1 and/or PD-L1 expression has been recently shown in preclinical studies, summarized in this review paper (Table 1).

A very illustrative finding, highlighting the power of whole-body imaging of protein expression, is the unexpected imaging signal reflecting expression of PD-L1 in brown fat cells [29–32], although its role in health and disease remains to be uncovered [33].

### Noninvasive molecular imaging of PD-1 and PD-L1 using mAbs: success and limitations

The clinical efficacy of mAbs as a therapeutic has prompted their evaluation as diagnostic tracers. Most of these studies have focused on assessing PD-L1 expression in the tumor environment.

**Table 1.** Overview of the imaging studies performed in preclinical models.

Probe name	Label	Timing	Targeting specificity	Tumor type	Therapeutic use?	Reference
Anti-PD-L1 mAbs						
PD-L1.3.1	<sup>111</sup> In	7 days	Human	Breast cancer	No	[34]
Atezolizumab	<sup>111</sup> In	3-5 days	Human	Breast cancer, NSCLC	Yes	[31]
	NIR					
10B5, 5H1	<sup>111</sup> In	3 days	Human	Breast cancer	No	[35]
10F.9G2	<sup>111</sup> In	1-3 days	Mouse	Melanoma	No	[29]
10F.9G2	<sup>111</sup> In	1-3 days	Mouse	Breast cancer	No	[36]
10F.9G2	<sup>64</sup> Cu	1 day	Mouse	Melanoma	No	[32]
Atezolizumab	<sup>64</sup> Cu	1-2 days	Human	Breast cancer	Yes	[39]
Not specified	<sup>89</sup> Zr	2 days	Mouse	Melanoma, head & neck cancer	No	[40]
Rec. huIgG (C4)	<sup>68</sup> Zr	48 hours	Mouse Human	Melanoma, NSCLC, prostate cancer	No	[41]
Anti-PD-1 mAbs						
eBioscience	<sup>64</sup> Cu	2 days	Mouse	Melanoma	No	[56]
RMP1-14	<sup>64</sup> Cu	1 day	Mouse	Melanoma	No	[32]
Pembrolizumab	<sup>89</sup> Zr	2 days	Human	Not applicable	Yes	[57]
Nivolumab	<sup>89</sup> Zr	8 days	Monkey	Not applicable	Yes	[58]
Nivolumab	<sup>89</sup> Zr	7 days	Mouse (humanized)	Adenocarcinoma	Yes	[59]
Pembrolizumab	<sup>89</sup> Zr/ <sup>64</sup> Cu	6/2 days	Mouse (humanized)	Melanoma	Yes	[60,61]
RMP1-14	<sup>64</sup> Cu	12 hours	Mouse	Breast cancer	No	[62,63]
Small PD-L1-binding moieties						
PD-1 variant	<sup>64</sup> Cu	1 hour	Mouse	Colorectal cancer	No	[65,66]
WL12	<sup>64</sup> Cu	1 hour	Human	CHO	No	[68,69]
sdAbs	<sup>99m</sup> Tc	1 hour	Mouse	Lung epithelial cancer	No	[30]
Affibody	<sup>18</sup> F	90 minutes	Human	LOX/SUDHL6 xenografts	No	[70]
Adnectin	<sup>18</sup> F	2 hours	Human Monkey	Lung adenocarcinoma	No	[71]

Abbreviations: CHO: Chinese hamster ovary; Cu: copper; In: indium; mAb: monoclonal antibody; NIR: near infrared; NSCLC: non-small cell lung cancer; sdAbs: single-domain Antibodies; Tc: technetium; Zr: zirconium.

Heskamp et al. were one of the first to provide evidence that noninvasive imaging of PD-L1 in the tumor with a mAb-tracer is technically possible [34]. They used an <sup>111</sup>In-labeled IgG1 mAb (PD-L1.3.1), which specifically and exclusively binds human PD-L1 with a nanomolar affinity. Imaging of xenografted PD-L1<sup>neg</sup> (MCF7) and PD-L1<sup>pos</sup> (MDA-MB-231) breast cancer cell lines was performed, showing specific uptake of the mAb in PD-L1-positive tumors, with tumor-to-blood ratios that increased over time and reached a maximum 7 days post injection. Intratumoral uptake of the <sup>111</sup>In-labeled anti-PD-L1 antibody was observed to be heterogeneous, with high signals in the periphery of the tumor. Also, Chatterjee et al. used an <sup>111</sup>In-labeled anti-PD-L1 mAb, the clinically used therapeutic atezolizumab, to evaluate PD-L1 expression in the tumor [31]. In addition, they used atezolizumab conjugated to a near-infrared dye. Atezolizumab is a humanized IgG1k mAb with high affinity for both human (0.43 nM) and mouse (0.13 nM) PD-L1. The cell lines used in this study showed no, low, intermediate or high human PD-L1 expression and included PD-L1-transfected Chinese hamster ovary (CHO), H2444, MDA-MB-231, SUM149, H1155 and untransfected CHO (ranked from high to low PD-L1 expression). *In vitro* binding studies and *in vivo* imaging studies showed uptake of the mAb consistent with PD-L1

expression. Also in this study, the uptake showed the best signal-to-noise ratios at 72 h (radiolabel) or 120 h (near infrared dye) post injection.

The previous studies were performed in xenografted immunodeficient mice, and, therefore, did not take into account potential expression of PD-L1 on immune cells. In contrast, Josefsson et al. performed imaging studies in breast cancer-bearing (NT2.5 or 4T1) immunocompetent mice using a high-affinity (8.3 nM) <sup>111</sup>In-DTPA-anti-mouse PD-L1 mAb (10B5, clone 5H1) [35]. Radioactivity peaked in the tumor at 72 h post injection, a time point at which the spleen, liver, thymus, heart and lungs also showed high radioactivity. mAb clearance from all organs, except for the tumor, spleen, liver and thymus, was seen at 144 h post injection. The expression of PD-L1 in the spleen, kidneys and thymus was confirmed with IHC. However, the low PD-L1 levels in the thymus assessed with IHC did not correlate with the high signals obtained through imaging. In a follow-up study, they also evaluated the effect of protein concentrations on the biodistribution of the <sup>111</sup>In-DTPA-anti-PD-L1 mAb in a PD-L1<sup>pos</sup> murine B16F10 melanoma model. They observed that by increasing the amount of mAb, tumor uptake also increases. They hypothesized that this is a result of high binding of excess antibody in the spleen, providing more radiolabeled antibody to the tumor, confirming their

previous results that the spleen serves as an antibody sink. A dose of 3 mg/kg antibody resulted in optimal biodistribution and tumor-to-background ratios. On SPECT imaging, tumor, spleen and liver were best visible at later and thymus at earlier time points [29].

Subsequently, imaging was used in a NT2.5 breast cancer model as a surrogate and possible companion diagnostic for targeted alpha-therapy with  $^{225}\text{Ac}$ -DOTA-labeled anti-PD-L1 antibody. It was concluded that alpha-therapy with this probe is not recommended due to its *in vivo* instability and undesired on- and off-target alpha-irradiation of spleen, liver, thymus and kidneys [36].

Hettich et al. studied the use of a PD-L1 mAb (clone 10F.9G2; BioXcell) labeled through NOTA with  $^{64}\text{Cu}$  [32]. They were the first to evaluate their tracer in PD-L1-deficient mice. The tracer showed specific uptake in spleen, lymph nodes, lungs, heart, thymus, intestines, pancreas, brown fat and kidneys in wild type mice, which was absent in knockout mice. To evaluate the tracer for tumor stratification, imaging was performed in mice bearing mouse PD-L1<sup>pos</sup> and PD-L1<sup>neg</sup> B16 melanoma. *In vivo* as well as *ex vivo* analysis of  $^{64}\text{Cu}$ -labeled mAb uptake revealed much higher signals in the PD-L1<sup>pos</sup> compared to the

PD-L1<sup>neg</sup> tumors (Figure 1). Furthermore, they performed PET imaging in IFN- $\gamma$ -treated PD-L1 wild type or knockout mice, as IFN- $\gamma$  is known to upregulate PD-L1. Uptake of the anti-PD-L1 mAb could be detected in the lungs, confirming that the lung is continuously exposed to high levels of antigens that induce IFN- $\gamma$  secreting lymphocytes [37]. Using flow cytometry, they showed that, in particular, non-leukocytes in the lung express PD-L1, indicating that anti-lung T-cell responses are strongly restrained by the PD-1:PD-L1 checkpoint pathway. The upregulation of PD-L1 on non-leukocytes in the lungs in response to IFN- $\gamma$  signifies the critical role of the PD-1 checkpoint as a means to escape the adaptive T-cell-mediated immune response and explains the response rate of around 20% after PD-1:PD-L1 blockade in lung cancer patients [38].

Atezolizumab was also evaluated after labeling with  $^{64}\text{Cu}$ . In analogy to the  $^{111}\text{In}$ -atezolizumab study that was described above [31], imaging of no, low, intermediate or high PD-L1-expressing tumors was performed, showing comparable results, i.e., uptake correlating to levels of PD-L1 expression in these tissues [39].

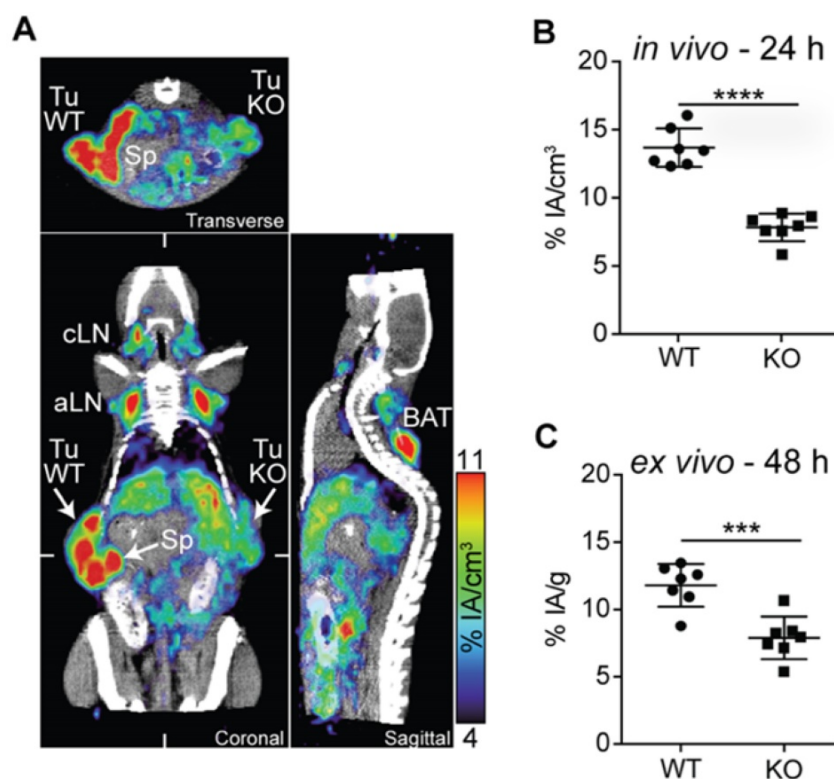


**Figure 1. PD-L1 immunoPET/CT in mice with WT and PD-L1 KO tumors.** (A) C57BL/6 mice were subcutaneously injected with  $2 \times 10^5$  B16F10 CD133 (left) and  $8 \times 10^5$  B16F10 CD133 PD-L1 KO tumor cells (right). Ten days later, mice were injected with  $^{64}\text{Cu}$ -NOTA-PD-L1 mAb ( $20 \mu\text{g}$ ;  $11.65 \pm 0.13 \text{ MBq}$ ), and 24 h later, representative coronal, transverse and sagittal immunoPET/CT scans were acquired. (B) *in vivo* and (C) *ex vivo* biodistribution of tracer uptake in WT and PD-L1 KO tumors ( $n = 7$ ). aLN: axillary lymph node; BAT: brown adipose tissue; cLN: cervical lymph node; Sp: spleen; Tu KO: PD-L1 KO tumor; Tu WT: wild-type tumor; Adapted with permission from [32], copyright 2016.

Using an  $^{89}\text{Zr}$ -labeled anti-mouse-PD-L1 mAb, upregulation of PD-L1, after radiotherapy alone or in combination with anti-PD-1 therapy, was monitored in head-and-neck squamous cell carcinoma and melanoma mouse models. PET/CT correlated to flow cytometry showed upregulation of PD-L1 in the irradiated tumors but not in the anti-PD-1-treated tumors [40].

Recently, an  $^{89}\text{Zr}$ -labeled recombinant human IgG (C4) that binds an extracellular epitope of PD-L1 was evaluated. C4 binds to human and mouse PD-L1 with a  $K_D$  of 4.2 nM and 0.34 nM, respectively. C4 is labeled to  $^{89}\text{Zr}$  through desferrioxamine B with high purity. The biodistribution of the radiotracer was evaluated in nude mice bearing PD-L1<sup>pos</sup> H1975 NSCLC cells using PET/CT, showing the highest tumor uptake at 48 h after injection. Furthermore, the tracer was evaluated in a patient-derived xenograft (PDX) obtained from NSCLC patients. PD-L1 expression on tissue was observed by immunofluorescence imaging. PET/CT images with  $^{89}\text{Zr}$ -C4 showed 10-fold higher uptake in PD-L1<sup>pos</sup> PDX compared to images with a heat-denatured  $^{89}\text{Zr}$ -C4. Furthermore, they evaluated PD-L1 expression in immunocompetent mice bearing PD-L1<sup>pos</sup> B16F10 tumor. As in the NSCLC model, tumor uptake was the highest 48 h after injection and signals in tumor, liver and spleen were suppressed by co-injection of an excess of unlabeled C4. Moreover, C4 was used to evaluate the impact of chemotherapy on PD-L1, as this is known to influence PD-L1 expression.

Therefore, immunodeficient mice bearing H1975 NSCLC tumors were treated with vehicle, taxol or doxorubicin for 3 days. Uptake was substantially higher in taxol-treated tumors compared to vehicle-treated, while it was decreased in doxorubicin-treated tumors. In contrast, in B16F10 tumors, doxorubicin had limited effect on tracer uptake but taxol increased radiotracer uptake [41].

As it has been shown that there is a correlation between the response to PD-1:PD-L1 therapy and the presence of tumor-infiltrating lymphocytes expressing PD-1 [42–55], imaging of PD-1 has also received attention, albeit to a lesser extent than imaging of PD-L1. Natarajan et al. evaluated a mouse anti-PD-1 mAb (eBioscience) radiolabeled with  $^{64}\text{Cu}$  through DOTA, showing efficient binding to PD-1<sup>pos</sup> cells both *in vitro* and *in vivo* [56]. The biodistribution of the radiotracer was studied using immuno-PET in B16 melanoma-bearing transgenic mice in which PD-1- and luciferase-expressing regulatory T cells are present in the tumor as well as in lymphoid organs like the spleen. Accumulation was observed at the tumor site after 48 h and could be significantly

reduced using an excess of unlabeled mAb, confirming the tracer's specificity for PD-1. As the transgenic regulatory T cells also express luciferase, bioluminescence imaging was performed, correlating the presence of luciferase-expressing regulatory T-cells in the tumor to the uptake of the radiotracer.

Also, Hettich et al. evaluated a  $^{64}\text{Cu}$ -labeled PD-1 mAb. First, they evaluated PD-1 expression on different cell types using flow cytometry, showing that only a small percentage of cells in the spleen and lymph nodes of healthy mice showed low expression of PD-1. These were primarily CD3<sup>pos</sup> T cells, of which the CD4<sup>pos</sup> fraction was more positive for PD-1 than the CD8<sup>pos</sup> fraction. Among the CD4<sup>pos</sup> PD-1<sup>pos</sup> T cells, half of them were regulatory T cells. Despite the low percentage of PD-1<sup>pos</sup> cells, PET imaging clearly detected PD-1 expression in both the spleen and lymph nodes in healthy wild type but not in PD-1 knockout mice 24 h post injection. In this study, imaging was also performed to follow PD-1 expression in B16 melanoma-bearing mice during the course of therapy with high-dose  $\gamma$ -irradiation and checkpoint-blocking mAbs. Tracer uptake was detected in the tumor, lymph nodes and spleen, with a substantially lower uptake in mice treated with the immune checkpoint-blocking therapy [32].

Recently, England et al. evaluated the FDA-approved mAb pembrolizumab, a humanized IgG4 mAb, using  $^{89}\text{Zr}$ -labeling for PET imaging [57]. The biodistribution was assessed in a mouse and rat model, showing non-specific accumulation in the blood pool, liver and spleen. Imaging in mice implanted with human peripheral blood mononuclear cells confirmed its specific binding to human PD-1<sup>pos</sup> T-cells in salivary glands. On the other hand, Cole *et al.* were the first to evaluate  $^{89}\text{Zr}$ -labeled FDA-approved anti-PD-1 mAb nivolumab for PET imaging in non-human primates. Nivolumab is a fully human IgG4 that binds with similarly high affinity (3 nM) to both human and cynomolgus PD-1. Nivolumab is conjugated with  $^{89}\text{Zr}$  through desferrioxamine (DFO). PET imaging in cynomolgus monkeys showed increasing spleen uptake over time, which could be reduced by injecting unlabeled nivolumab, suggesting specificity for PD-L1<sup>pos</sup> dendritic cells in the spleen. Similarly, tracer uptake in the lymph nodes increased over time, attributed to binding to PD-1<sup>pos</sup> lymphocytes. Non-specific bone uptake was also observed, due to release of  $^{89}\text{Zr}$  from the DFO chelator [58].

England *et al.* also developed and characterized an anti-PD-1 PET tracer ( $^{89}\text{Zr}$ -Df-nivolumab) to image the biodistribution of PD-1-expressing T-cell infiltrates using a humanized murine model of lung cancer.

Using humanized A549 tumor-bearing mice, they observed a specific outlining of subcutaneous tumors through targeting of localized activated T-cells expressing PD-1 in the tumors by their tracer. The maximum tumor uptake values of  $9.85 \pm 2.73$  %ID/g were reached at 168 h post injection. In addition to tumor uptake, infiltration of T cells in the salivary and lacrimal gland was noticeably visible and confirmed using histological analysis. They validated the imaging results by *ex vivo* biodistribution studies and immunohistochemistry [59]. In conclusion, data generated by England *et al.* show that PD-1-targeted tumor imaging *in vivo* may assist in disease diagnostics, patient stratification, disease monitoring and the design and development of new immunotherapies.

Natarjan *et al.* published a study using the anti-PD-1 mAb pembrolizumab radiolabeled with the positron emitter  $^{89}\text{Zr}$  or  $^{64}\text{Cu}$ . They imaged the PD-1 status of human peripheral blood mononuclear cells (PBMCs) adoptively transferred to NSG mice bearing A375 human skin melanoma tumors. Their observations demonstrate the specific imaging of human PD-1-expressing TILs within the tumor and lymphoid tissues. Results suggest that PET can be used for noninvasive detection of PD-1 *in vivo* and could be clinically translatable to, for example, monitor response to IC blockade therapy in cancer patients [60,61].

Finally, Du *et al.* recently developed a novel PD-1-targeting strategy where IRDye800CW- and  $^{64}\text{Cu}$ -labeled liposomes, loaded with doxorubicin (DOX), were conjugated with an PD-1 antibody and evaluated for *in vivo* cancer imaging and therapy. 4T1 breast tumor-bearing mice were successfully visualized with PD-1-Liposome-DOX- $^{64}\text{Cu}$ /IRDye800CW using NIRE/PET imaging. They also observed that tumor growth was significantly inhibited in the PD-1-Liposome-DOX-treated group than the IgG control. More recently, the same group published a study that demonstrates the feasibility of using the same PD-1-IRDye800CW-conjugated liposomes for image-guided tumor resection [62,63].

These studies collectively show that mAbs can be used to detect PD-1 or PD-L1 in tumors irrespective of the radiolabel ( $^{111}\text{In}$ ,  $^{64}\text{Cu}$  and  $^{89}\text{Zr}$ ). However, these studies also show that mAb-mediated imaging is confronted with some limitations, which are largely due to the size of the mAbs. They are not cleared rapidly from the blood, and they are less proficient in penetrating tissues like tumors [45,64]. Consequently, imaging with mAbs is associated with considerable background signals and a need to perform the imaging several days after injection of the mAbs to obtain the best contrast image. Moreover, as the mAbs

are labeled with radioactivity, the radiation burden to highly perfused and radiosensitive organs is high. Therefore, other probes with a smaller size, and thus rapid clearance and high tissue penetration profile, have been evaluated for the purpose of imaging PD-L1.

### Noninvasive molecular imaging of PD-L1 using small PD-L1-binding moieties

Several PD-L1-binding moieties with a size that is considerably smaller than that of mAbs have been assessed to image PD-L1 in the tumor environment, including engineered PD-1 ectodomains, peptides, nanobodies, affibodies and adnectins.

The ectodomain of human PD-1 has been shown to block human PD-L1 binding and has been used by Maute *et al.* for imaging of human PD-L1 [65]. A high-affinity consensus (HAC) domain was selected from a randomized PD-1 ectodomain library and used to create a microbody by fusing them to the dimeric CH3 domain of human IgG1.

This microbody and, for comparison, an anti-PD-L1 mAb were fluorescently labeled and used for imaging of mice bearing CT26 colorectal cancer cells. Fluorescence microscopy and flow cytometry were used to detect binding to PD-L1<sup>pos</sup> tumor cells, showing that both the mAb and microbody bound PD-L1 with high specificity. As expected, based on the lower capacity of mAbs to penetrate tumor tissue, it was shown, using fluorescence microscopy, that the mAb binds PD-L1 at the periphery of the tumor, while the microbody was better dispersed throughout the tumor. The  $^{64}\text{Cu}$ -labeled microbody showed a high tumor-to-muscle and tumor-to-blood signal in the human PD-L1<sup>pos</sup> tumor as early as one hour after injection. However, nonspecific signals were seen in the salivary glands, lymph nodes and spleen. The high signal obtained in the kidneys reflects its rapid urinary clearance. To follow up on this imaging study, glycosylated and aglycosylated HAC domains (without IgG3-CH3) were labeled with  $^{64}\text{Cu}$  or  $^{68}\text{Ga}$ . Aglycosylation had an impact on biodistribution with lower nonspecific signals in the salivary gland, spleen and lymph nodes but longer blood circulation. Further research needs to be done to evaluate how much of this signal was due to free metal and to decreased circulation time in the blood.

This study further showed that the signal-to-noise ratio was decreased when  $^{64}\text{Cu}$  was replaced with  $^{68}\text{Ga}$  [66]. Besides its diagnostic value, the binding of the ectodomain of PD-1 to PD-L1 also had therapeutic value [65]. Such therapeutic value was also shown for the ectodomain of PD-L1, which can interfere with the PD-1:PD-L1 pathway through the binding of PD-1 [67]. This suggests that this

ectodomain is also amenable for imaging studies in which PD-1 is the target.

Another small binding moiety that has been evaluated for imaging is the  $^{64}\text{Cu}$ -labeled WL12 peptide, which binds with low nM affinity to human but not to mouse PD-L1. Specificity was confirmed *in vitro* and *in vivo* using PD-L1-transfected CHO cells, showing specific tumor uptake as early as 10 min after injection of the radiotracer, which was, however, optimal at 1 h. The tumor uptake was retained up to 120 min, although high nonspecific signals in liver and kidneys were also observed [68,69].

Also, single-domain antibodies (sdAbs), often referred to as nanobodies, have been evaluated for SPECT/CT imaging in syngeneic mouse tumor models with varying PD-L1 expressions [30]. Nanobodies are 15 kDa antigen-binding fragments of heavy-chain-only antibodies found in camelids. In this study, four nanobodies with nanomolar affinity for mouse PD-L1 were labeled with  $^{99\text{m}}\text{Tc}$  and used in

SPECT/CT to evaluate their biodistribution in immunocompetent wild type and PD-L1 knockout mice as well as in mice bearing TC-1 lung epithelioma with no, low or high PD-L1 expression. Imaging was performed one hour after injection, showing high signal-to-noise ratios and PD-L1-specific signal in tumors, lungs, heart, thymus, spleen, lymph nodes and brown adipose tissue. Nanobodies are cleared from the blood via the urinary tract, resulting in high kidney signals [30]. SPECT/CT images followed by flow cytometry-based assessment of the PD-L1 levels on immune cells (CD45<sup>pos</sup>) and non-immune cells (CD45<sup>neg</sup>) in the tumors showed that the uptake was correlated to the expression levels of PD-L1 in these tumors (Figure 2). Uptake in tumors was shown to be patchy, highlighting the heterogeneity of PD-L1 expression in the tumor and underlining the necessity of mapping the PD-L1 expression in the entire tumor instead of biopsies.

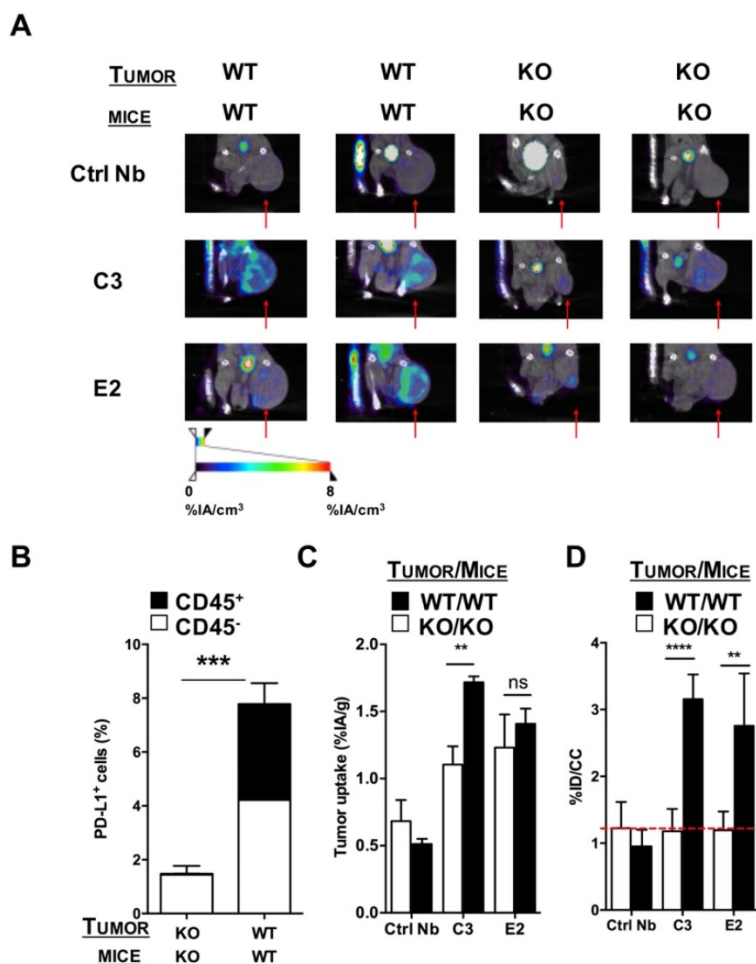


**Figure 2.** SPECT/CT in a PD-L1 KO TC-1 model 1 h after injection of  $^{99\text{m}}\text{Tc}$ -labeled nanobodies C3 or E2. **(A)** Images of the SPECT/CT scans to evaluate  $^{99\text{m}}\text{Tc}$ -C3 and E2 for tumor stratification in PD-L1 KO mice bearing PD-L1 KO TC-1 tumors (KO) or mice bearing wild type, PD-L1<sup>pos</sup> TC-1 tumors (WT) (n=6). The red arrows indicate the tumors on the images. **(B)** Ex vivo PD-L1 expression on cancer cells (CD45<sup>neg</sup>, white bar) and tumor-infiltrating immune cells (CD45<sup>pos</sup>, black bar) of PD-L1 KO tumors injected in PD-L1 KO mice and WT TC-1 cells injected in WT mice, was evaluated by flow cytometry. The graph summarizes the percentage of PD-L1 as mean  $\pm$  SEM (n=6). **(C)** Results of the gamma counting of isolated organs from PD-L1 KO mice bearing PD-L1 KO tumors (KO, white bars) or WT mice bearing WT (PD-L1<sup>pos</sup>) tumors (WT, black bars) injected with  $^{99\text{m}}\text{Tc}$ -C3 or -E2. The graph summarizes the %IA/g as mean  $\pm$  SEM (n=6). **(D)** Tumor uptake (%ID/cc) calculated via region of interest analysis on the periphery of the tumor from PD-L1 KO mice bearing PD-L1 KO tumors (KO, white bars) or WT mice bearing PD-L1<sup>pos</sup> tumors (WT, black bars) injected with  $^{99\text{m}}\text{Tc}$ -C3 and E2. The graph summarizes the %ID/cc as mean  $\pm$  SEM (n=6). Adapted with permission from [30], copyright 2017.

Another small protein that has been evaluated for imaging of PD-L1 is the affibody molecule NOTA-Z<sub>PD-L1\_1</sub>. It is based on a 58 amino acid scaffold protein, from which high-affinity PD-L1 binders were selected using phage-display, and has affinities of 1 nM for human and rhesus PD-L1. It is labeled with Al<sup>18</sup>F through maleimide coupling of NOTA. Using PET imaging and *ex vivo* biodistribution measurements in PD-L1<sup>pos</sup> tumors, specificity was confirmed. Blood clearance happened quickly, with tumor-to-blood ratios >5 achieved as early as 90 min after injection. Uptake in non-tumor tissues was low, with the highest signals in kidney and bladder, reflecting excretion, but also in liver, which showed non-negligible uptake of the radiotracer. *Ex vivo* autoradiography of mixed PD-L1<sup>pos</sup> and PD-L1<sup>neg</sup> tumors showed heterogeneous uptake, with areas of highest radiotracer uptake corresponding to PD-L1 positivity on IHC [70].

On the other hand, Donnelly *et al.* evaluated <sup>18</sup>F-labeled anti-PD-L1 Adnectin (<sup>18</sup>F-BMS-986192) uptake in PD-L1<sup>pos</sup> and PD-L1<sup>neg</sup> tumors in mice, as well as in healthy cynomolgus monkeys. Adnectins are derived from the 10<sup>th</sup> type III domain of human fibronectin, which resembles the variable domains of an antibody, and have two sets of antiparallel beta sheets with solvent-accessible loops at each pole. The generated Adnectin has a size of 10 kDa and binds with 35 pM dissociation constants to both human and cynomolgus but not to murine PD-L1. *In vitro* radioligand binding studies and autoradiography of L2987 PD-L1<sup>pos</sup>- and HT-29 PD-L1<sup>neg</sup>-xenografted tumors and patient NSCLC tumor samples showed specific binding of <sup>18</sup>F-BMS-986192. Furthermore, using PET imaging and *ex vivo* biodistribution studies, they showed higher uptake of the radiolabeled adnectin in L2987 PD-L1<sup>pos</sup> tumors than in PD-L1<sup>neg</sup> tumors, with a plateau between 90-120 min post injection. Uptake in peripheral organs was moderate as was uptake in muscle. The only tissue showing high uptake was the kidney, reflecting clearance. PET imaging in healthy cynomolgus monkeys showed accumulation in the spleen, while overall background signals were low. PD-L1 positivity in the spleen was confirmed with IHC [71].

These studies show that several alternatives for mAbs for imaging of PD-L1 are under development. These alternatives have the advantage that the size of the tracer is small and, as a consequence, the tracer can penetrate into the core of tumors, while the unbound tracer is rapidly cleared via the kidneys. The latter implies that imaging can be performed in a matter of minutes to hours and that the patient is only exposed to radioactivity for a limited amount of time.

## Perspectives on the predictive value of PD-1 and PD-L1 expression in the tumor environment in a clinical setting

Since the regulatory approval of PD-1 and PD-L1 immune checkpoint inhibitors, the search for a predictive method to guide patient selection has emerged. Patient selection will avoid ineffective treatment of patients and limit the number of patients harmed by the potential autoimmune side effects related to blocking of the PD-1:PD-L1 axis [15].

To date IHC is used to determine the PD-1:PD-L1 status of the tumor. This is, however, confounded by various unresolved issues, such as the use of biopsies from primary versus metastatic lesions, the variety in detection antibodies, tissue preparation and staining procedures, and detection cut-offs, which is further thwarted by the decision to discriminate detection of PD-L1 on tumor cells versus immune cells. Moreover, expression levels of PD-L1 on tumors that are classically associated with clinical response widely range from 14% to 100%, while there are cases of robust responses amongst patients with no expression, at least according to IHC analysis [10,11,72,73]. In percentages, this translates to a response rate for PD-L1<sup>pos</sup> tumors of 48%, compared to 15% amongst PD-L1<sup>neg</sup> tumors [27].

The development of a noninvasive molecular imaging strategy to evaluate PD-L1 expression *in situ* resolves the practical issues encountered with IHC. Moreover, molecular imaging offers the advantage that it provides a full picture on the status of the tumor environment, although without discriminating tumor cells from immune cells. Molecular imaging could be used as a guide to make informed decisions at the start of the therapy. As molecular imaging can be repeated over time, follow-up of the PD-L1 status during the course of treatment is feasible, thereby aiding decisions to continue or stop PD-1:PD-L1 blockade therapy, or to add it to an ongoing treatment. As such, nuclear medicine could be exploited to rationally design a personalized immunotherapy regimen. Nonetheless, further studies are required to validate that expression of PD-L1 (and/or PD-1) as assessed by molecular imaging serves to predict therapy response.

## Challenges for clinical translation

A PD-1 or PD-L1 detecting radiotracer that is developed for molecular imaging should fulfill several requirements to be of clinical value. First of all, its use should significantly improve patient outcome and change therapeutic conduct, which in a way is directly linked to the outstanding question of whether PD-1 or PD-L1 are good biomarkers.

The radiotracer should at least provide additional evidence for the selection of patients or, even better, be superior to the currently available strategies to detect PD-1:PD-L1 expression in the tumor environment.

To date, IHC is the method of choice to determine the expression of PD-L1, and is already a companion diagnostic for PD-(L)1 drugs in most lung cancer patients. As discussed above, IHC withholds several practical challenges and ignores the heterogeneity of the tumor environment. It is contended that any probe, be it an antibody, peptide, nanobody, microbody, affibody or adnectin, is more informative, as it provides an image of the entire tumor, both primary and metastatic, albeit without information on the cell type expressing PD-1 or PD-L1.

Given the existing companion diagnostics, imaging might first become a complementary diagnostic that could in time evolve into a true companion diagnostic in specific disease settings and for specific geographical areas [74]. It is likely that smaller proteins like affibodies, microbodies, nanobodies or peptides will be of more relevance as these can reach the core of tumors, while antibodies may be more limited in their tissue penetrating capacity due to their size. Initial clinical data, although still preliminary presented in a poster presentation, comparing  $^{89}\text{Zr}$ -Nivolumab with  $^{18}\text{F}$ -anti-PD-L1 adnectin in 10 lung cancer patients, seem to support this hypothesis, given the tracer uptake was only significantly higher in PD-L1-positive patients using the small compound [75]. These data also confirmed the safety and

feasibility of both mAb-based and adnectin-based PET imaging procedures in patients.

Another requirement for clinical translation is that the implementation of the radiotracer in the workflow should be easy. Especially in this context, antibodies are of less interest when compared to smaller proteins as it takes several days before high-contrast images can be generated. This is not an issue with smaller radiotracers that allow molecular imaging in a matter of hours [76]. Moreover, these proteins typically reduce the radiation burden to the patient given their rapid clearance and the use of shorter-lived isotopes. **Figure 3** summarizes the modalities that are currently available to detect PD-1 or PD-L1 expression in tumors, highlighting their advantages and disadvantages.

For translation, the radiotracer should be regulation-compatible, and this requires 'Good Manufacturing Practices' (GMP) in most Western countries. GMP production is costly, and since clinically used therapeutic agents are already available in GMP form, it is often less costly to use these as clinical imaging tracers. For others, in particular the requirements for radiological and pharmaceutical safety as well as GMP production might be more challenging. We are nevertheless convinced that the widespread application of PD-1- and PD-L1-targeting radiotracers could benefit many cancer patients. Therefore, large clinical trials are first needed to provide convincing evidence that assessment of PD-1 and/or PD-L1 in the tumor environment using molecular imaging is predictive for the therapy response. **Table 2** summarizes the currently ongoing clinical trials for image-based PD-1 and PD-L1 assessment.

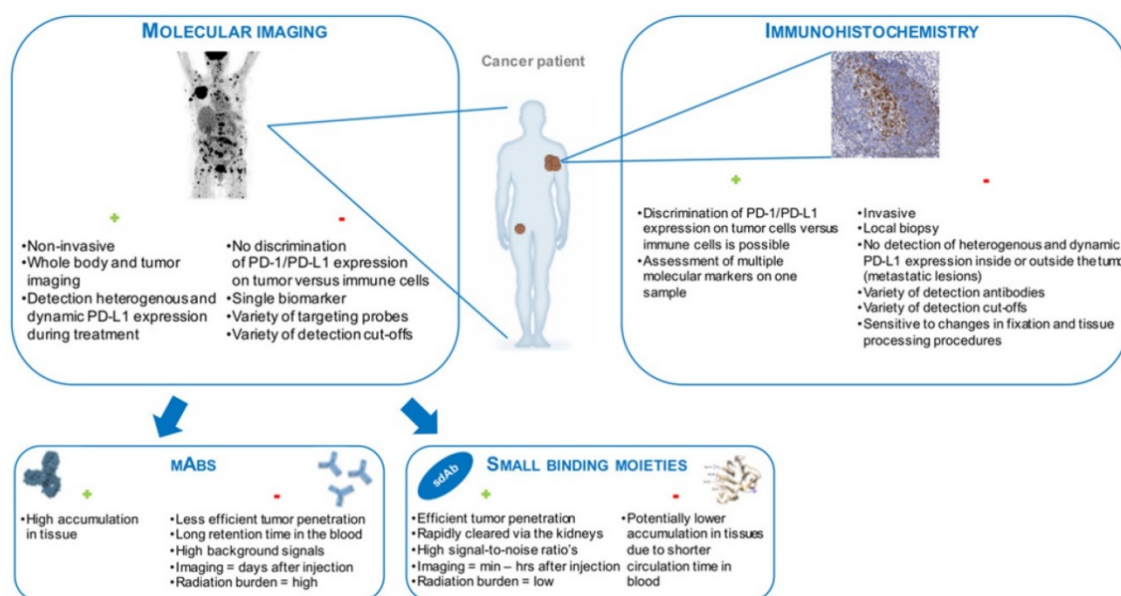


**Figure 3.** Schematic representation of the modalities that are currently available to detect PD-1 or PD-L1 expression in tumors, highlighting their advantages (+) and disadvantages (-).

**Table 2.** Overview of clinical trials on noninvasive imaging of PD-1:PD-L1.

Probe	Label	Phase	Tumor type	Patients	Location	End	NCT n°	EUDRACT
Pembrolizumab	<sup>89</sup> Zr	Phase II	NSCLC	N=10	Amsterdam, NL	Dec '19	NCT03065764	2015-004260-10
Atezolizumab	<sup>89</sup> Zr	Phase I	Breast, bladder, NSCLC	N=30	Groningen, NL	Jul '17	NCT02453984	2015-000996-29
Pembrolizumab	<sup>89</sup> Zr	Phase I/II	Melanoma, NSCLC	N=21	Groningen, NL	Jul '17	NCT02760225	2016-000941-30
Anti-PD-L1 Adnectin	<sup>18</sup> F	Substudy of Phase III	Melanoma	unknown	Amsterdam, NL	Apr '22		2015-004920-67 monocenter substudy
Anti-PD-L1 Adnectin	<sup>18</sup> F	Feasibility	NSCLC	N=10	Amsterdam, NL	Aug '18		2015-004760-11
Nivolumab	<sup>89</sup> Zr							
Durvalumab	<sup>89</sup> Zr	Feasibility	NSCLC	N=10	Amsterdam, NL	Jul '20		2015-005765-23
Anti-PD-L1 Nb	<sup>99m</sup> Tc	Phase I	NSCLC	N=50	Shanghai, CHN	Dec '18	NCT02978196	

Abbreviations: CHN: China; mAb: monoclonal antibody; Nb: nanobody; NL: the Netherlands; NSCLC: non-small cell lung cancer; Tc: technetium; Zr: zirconium

## Conclusion

In this review, a comprehensive overview is given on the state-of-the-art exploration of nuclear medicine to map PD-1 and PD-L1 expression. We discussed novel PD-1- and PD-L1-binding moieties, including microbodies, nanobodies and peptides, and the properties that make them interesting candidates as companion diagnostics, which in the near future might change how immune checkpoint blocking therapies are applied, to the benefit of many patients.

## Abbreviations

GMP: good manufacturing practice; IHC: immunohistochemical staining; mAb: monoclonal antibody; NSCLC: non-small cell lung cancer; PD-1: programmed cell death-1; PD-L1: programmed cell death-ligand 1 PD-L1<sup>pos</sup>: PD-L1 expressing; PD-L1<sup>neg</sup>: PD-L1 non-expressing; sdAb: single-domain antibody.

## Acknowledgements

This work was performed with the financial support of the Agency of Innovation by Science and Technology (IWT-SBO), "Kom op tegen Kanker (Stand up to Cancer), the Flemish cancer society" and the Melanoma Research Alliance. Broos K. is funded via an IWT-SB fellowship. Lecocq Q. is funded via an 'Emmanuel van der Schueren' fellowship and a FWO-SB fellowship. Keyaerts M. is a senior clinical investigator of the Research Foundation-Flanders.

Broos K., Lecocq Q., Keyaerts M., Raes G., Devoogdt N., and Breckpot K. contributed to the concept and design of the review. Furthermore, they contributed to the drafting and revision of the preview and the final approval of the version to be published. The authors declare that there is no conflict of interest regarding the publication of this article.

## Competing Interests

Keyaerts M. has received travel and accommodation expenses from Bayer NV; Devoogdt N. and Raes G. are co-founders of CamellIDs.

Devoogdt N. has received funding from Boehringer-Ingelheim, Complix. Broos K., Lecocq Q., Raes G. Devoogdt N., Keyaerts M. and Breckpot K. have patents on Nanobody imaging and therapy.

## References

- Lohmueller J, Finn OJ. Current modalities in cancer immunotherapy: Immunomodulatory antibodies, CARs and vaccines. *Pharmacol Ther.* 2017; 178: 31-47.
- Topalian SL, Drake CG, Pardoll DM. Immune checkpoint blockade: a common denominator approach to cancer therapy. *Cancer Cell.* 2015; 27: 450-61.
- Sharma P, Allison JP. The future of immune checkpoint therapy. *Science.* 2015; 348: 56-61.
- Zou W, Chen L. Inhibitory B7-family molecules in the tumour microenvironment. *Nat Rev Immunol.* 2008; 8: 467-77.
- Taube JM, Anders RA, Young GD, Xu H, Sharma R, McMiller TL, et al. Colocalization of inflammatory response with B7-h1 expression in human melanocytic lesions supports an adaptive resistance mechanism of immune escape. *Sci Transl Med.* 2012; 4: 127ra37.
- De Vlaeminck Y, Gonzalez-Rascon A, Goyvaerts C, Breckpot K. Cancer-Associated Myeloid Regulatory Cells. *Front Immunol.* 2016; 7: 113.
- Arasanz H, Gato-Canas M, Zuazo M, Ibanez-Vea M, Breckpot K, Kochan G, et al. PD1 signal transduction pathways in T cells. *Oncotarget.* 2017; 8: 51936-45.
- Weber JS, D'Angelo SP, Minor D, Hodi FS, Gutzmer R, Neyns B, et al. Nivolumab versus chemotherapy in patients with advanced melanoma who progressed after anti-CTLA-4 treatment (CheckMate 037): a randomised, controlled, open-label, phase 3 trial. *Lancet Oncol.* 2015; 16: 375-84.
- Robert C, Long G V, Brady B, Dutriaux C, Maio M, Mortier L, et al. Nivolumab in previously untreated melanoma without BRAF mutation. *N Engl J Med.* 2015; 372: 320-30.
- Powles T, Eder JP, Fine GD, Braiteh FS, Loriot Y, Cruz C, et al. MPDL3280A (anti-PD-L1) treatment leads to clinical activity in metastatic bladder cancer. *Nature.* 2014; 515: 558-62.
- Herbst RS, Soria J-C, Kowanetz M, Fine GD, Hamid O, Gordon MS, et al. Predictive correlates of response to the anti-PD-L1 antibody MPDL3280A in cancer patients. *Nature.* 2014; 515: 563-7.
- Larkin J, Chiarion-Sileni V, Gonzalez R, Grob JJ, Cowey CL, Lao CD, et al. Combined Nivolumab and Ipilimumab or Monotherapy in Untreated Melanoma. *N Engl J Med.* 2015; 373: 23-34.
- Brahmer J, Reckamp KL, Baas P, Crino L, Eberhardt WEE, Poddubskaya E, et al. Nivolumab versus Docetaxel in Advanced Squamous-Cell Non-Small-Cell Lung Cancer. *N Engl J Med.* 2015; 373: 123-35.
- Motz GT, Coukos G. Deciphering and reversing tumor immune suppression. *Immunity.* 2013; 39: 61-73.
- Hamid O, Robert C, Daud A, Hodi FS, Hwu W-J, Kefford R, et al. Safety and tumor responses with lambrolizumab (anti-PD-1) in melanoma. *N Engl J Med.* 2013; 369: 134-44.
- Aguiar PNJ, Perry LA, Penny-Dimri J, Babiker H, Tadokoro H, de Mello RA, et al. The effect of PD-L1 testing on the cost-effectiveness and economic impact of immune checkpoint inhibitors for the second-line treatment of NSCLC. *Ann Oncol.* 2017; 28: 2256-63.
- Alsaab HO, Sau S, Alzhrani R, Tatiparti K, Bhise K, Kashaw SK, et al. PD-1 and PD-L1 Checkpoint signaling inhibition for cancer immunotherapy: mechanism, combinations and clinical outcome. *Front Pharmacol.* 2017; 8.
- Wong ANM, McArthur GA, Hofman MS, Hicks RJ. The advantages and challenges of using FDG PET/CT for response assessment in melanoma in the era of targeted agents and immunotherapy. *Eur J Nucl Med Mol Imaging.* 2017; 44: 67-77.
- Seith F, Forschner A, Schmidt H, Pfannenber C, Guckel B, Nikolaou K, et al. 18F-FDG-PET detects complete response to PD1-therapy in melanoma patients two weeks after therapy start. *Eur J Nucl Med Mol Imaging.* 2018; 45: 95-101.
- Derclé L, Seban R-D, Lazarovici J, Schwartz LH, Houot R, Ammari S, et al. (18)F-FDG PET and CT scans detect new imaging patterns of response and

- progression in patients with Hodgkin Lymphoma treated by anti-Programmed Death 1 immune checkpoint inhibitor. *J Nucl Med.* 2018; 59: 15-24.
21. Derclé L, Ammari S, Seban R-D, Schwartz LH, Houot R, Labaied N, et al. Kinetics and nadir of responses to immune checkpoint blockade by anti-PD1 in patients with classical Hodgkin lymphoma. *Eur J Cancer.* 2018; 91: 136-44.
  22. Topalian SL, Hodi FS, Brahmer JR, Gettinger SN, Smith DC, McDermott DF, et al. Safety, activity, and immune correlates of anti-PD-1 antibody in cancer. *N Engl J Med.* 2012; 366: 2443-54.
  23. Yarchoan M, Hopkins A, Jaffee EM. Tumor mutational burden and response rate to PD-1 Inhibition. *N Engl J Med.* 2017; 377: 2500-1.
  24. Tang H, Liang Y, Anders RA, Taube JM, Qiu X, Mulgaonkar A, et al. PD-L1 on host cells is essential for PD-L1 blockade-mediated tumor regression. *J Clin Invest.* 2018; 128: 580-8.
  25. Hirsch FR, McElhinny A, Stanforth D, Ranger-Moore J, Jansson M, Kulangara K, et al. PD-L1 immunohistochemistry assays for lung cancer: Results from Phase 1 of the Blueprint PD-L1 IHC assay Comparison project. *J Thorac Oncol.* 2017; 12: 208-22.
  26. Grigg C, Rizvi NA. PD-L1 biomarker testing for non-small cell lung cancer: truth or fiction? *J Immunother cancer.* 2016; 4: 48.
  27. Sunshine J, Taube JM. PD-1/PD-L1 inhibitors. *Curr Opin Pharmacol.* 2015; 23: 32-8.
  28. Daud AI, Loo K, Pauli ML, Sanchez-Rodriguez R, Sandoval PM, Taravati K, et al. Tumor immune profiling predicts response to anti-PD-1 therapy in human melanoma. *J Clin Invest.* 2016; 126: 3447-52.
  29. Nedrow JR, Josefsson A, Park S, Ranka S, Roy S, Sgouros G. Imaging of Programmed Cell Death Ligand 1: Impact of protein concentration on distribution of anti-PD-L1 SPECT agents in an immunocompetent murine model of melanoma. *J Nucl Med.* 2017; 58: 1560-6.
  30. Broos K, Keyaerts M, Lecocq Q, Remmans D, Nguyen T, Escors D, et al. Non-invasive assessment of murine PD-L1 levels in syngeneic tumor models by nuclear imaging with nanobody tracers. *Oncotarget.* 2017; 8: 41932-46.
  31. Chatterjee S, Lesniak WG, Gabrielson M, Lisok A, Wharram B, Sysa-Shah P, et al. A humanized antibody for imaging immune checkpoint ligand PD-L1 expression in tumors. *Oncotarget.* 2016; 7: 10215-27.
  32. Hettich M, Braun F, Bartholomä MD, Schirmbeck R, Niedermann G. High-resolution PET imaging with therapeutic antibody-based PD-1/PD-L1 checkpoint tracers. *Theranostics.* 2016; 6: 1629-1640.
  33. Ingram JR, Dougan M, Rashidian M, Knoll M, Keliher EJ, Garrett S, et al. PD-L1 is an activation-independent marker of brown adipocytes. *Nat Commun.* 2017; 8: 647.
  34. Heskamp S, Hobo W, Molkenboer-Kuennen JDM, Olive D, Oyen WJG, Dolstra H, et al. Noninvasive imaging of tumor PD-L1 expression using radiolabeled anti-PD-L1 antibodies. *Cancer Res.* 2015; 75: 2928-36.
  35. Josefsson A, Nedrow JR, Park S, Banerjee SR, Rittenbach A, Jammes F, et al. Imaging, biodistribution, and dosimetry of radionuclide-labeled PD-L1 antibody in an immunocompetent mouse model of breast cancer. *Cancer Res.* 2016; 76: 472-9.
  36. Nedrow JR, Josefsson A, Park S, Back T, Hobbs RF, Brayton C, et al. Pharmacokinetics, microscale distribution, and dosimetry of alpha-emitter-labeled anti-PD-L1 antibodies in an immune competent transgenic breast cancer model. *EJNMMI Res.* 2017; 7: 57.
  37. The lungs at the frontlines of immunity. *Nature immunology.* 2015; 16: 17.
  38. Hellmann MD, Ott PA, Zugazagoitia J, Ready NE, Hann CL, De Braud FG, et al. Nivolumab (nivo) ± ipilimumab (ipi) in advanced small-cell lung cancer (SCLC): First report of a randomized expansion cohort from CheckMate 032. *J Clin Oncol.* 2017; 35: 8503.
  39. Lesniak WG, Chatterjee S, Gabrielson M, Lisok A, Wharram B, Pomper MG, et al. PD-L1 detection in tumors using [(64)Cu]Atezolizumab with PET. *Bioconjug Chem.* 2016; 27: 2103-10.
  40. Kikuchi M, Clump DA, Srivastava RM, Sun L, Zeng D, Diaz-Perez JA, et al. Preclinical immunoPET/CT imaging using Zr-89-labeled anti-PD-L1 monoclonal antibody for assessing radiation-induced PD-L1 upregulation in head and neck cancer and melanoma. *Oncimmunology.* 2017; 6.
  41. Truillet C, Oh HJ, Yeo SP, Lee C-Y, Huynh LT, Wei J, et al. Imaging PD-L1 expression with ImmunoPET. *Bioconjug Chem.* 2018; 29: 96-103.
  42. Ahmadzadeh M, Johnson LA, Heemskerk B, Wunderlich JR, Dudley ME, White DE, et al. Tumor antigen-specific CD8 T cells infiltrating the tumor express high levels of PD-1 and are functionally impaired. *Blood.* 2009; 114: 1537-44.
  43. Chapon M, Randriamampita C, Maubec E, Badoual C, Fouquet S, Wang S-F, et al. Progressive upregulation of PD-1 in primary and metastatic melanomas associated with blunted TCR signaling in infiltrating T lymphocytes. *J Invest Dermatol.* 2011; 131: 1300-7.
  44. French JD, Kotnis GR, Said S, Raeburn CD, McIntyre RCJ, Klopper JP, et al. Programmed death-1+ T cells and regulatory T cells are enriched in tumor-involved lymph nodes and associated with aggressive features in papillary thyroid cancer. *J Clin Endocrinol Metab.* 2012; 97: 934-43.
  45. Lee CM, Tannock IF. The distribution of the therapeutic monoclonal antibodies cetuximab and trastuzumab within solid tumors. *BMC Cancer.* 2010; 10: 255.
  46. Matsuzaki J, Gnjjatic S, Mhawech-Fauceglia P, Beck A, Miller A, Tsuji T, et al. Tumor-infiltrating NY-ESO-1-specific CD8+ T cells are negatively regulated by LAG-3 and PD-1 in human ovarian cancer. *Proc Natl Acad Sci U S A.* 2010; 107: 7875-80.
  47. Muenst S, Soysal SD, Gao F, Obermann EC, Oertli D, Gillanders WE. The presence of programmed death 1 (PD-1)-positive tumor-infiltrating lymphocytes is associated with poor prognosis in human breast cancer. *Breast Cancer Res Treat.* 2013; 139: 667-76.
  48. Scott AM, Wolchok JD, Old LJ. Antibody therapy of cancer. *Nat Rev Cancer.* 2012; 12: 278-87.
  49. Sfianos KS, Bruno TC, Meeker AK, De Marzo AM, Isaacs WB, Drake CG. Human prostate-infiltrating CD8+ T lymphocytes are oligoclonal and PD-1+. *Prostate.* 2009; 69: 1694-703.
  50. Sun S, Fei X, Mao Y, Wang X, Garfield DH, Huang O, et al. PD-1(+) immune cell infiltration inversely correlates with survival of operable breast cancer patients. *Cancer Immunol Immunother.* 2014; 63: 395-406.
  51. Zhang Y, Huang S, Gong D, Qin Y, Shen Q. Programmed death-1 upregulation is correlated with dysfunction of tumor-infiltrating CD8+ T lymphocytes in human non-small cell lung cancer. *Cell Mol Immunol.* 2010; 7: 389-95.
  52. Shi F, Shi M, Zeng Z, Qi R-Z, Liu Z-W, Zhang J-Y, et al. PD-1 and PD-L1 upregulation promotes CD8(+) T-cell apoptosis and postoperative recurrence in hepatocellular carcinoma patients. *Int J cancer.* 2011; 128: 887-96.
  53. Taube JM, Klein A, Brahmer JR, Xu H, Pan X, Kim JH, et al. Association of PD-1, PD-1 ligands, and other features of the tumor immune microenvironment with response to anti-PD-1 therapy. *Clin Cancer Res.* 2014; 20: 5064-74.
  54. Grosso J, Horak CE, Inzunza D, Cardona DM, Simon JS, Gupta AK, et al. Association of tumor PD-L1 expression and immune biomarkers with clinical activity in patients (pts) with advanced solid tumors treated with nivolumab (anti-PD-1; BMS-936558; ONO-4538). *J Clin Oncol.* 2013; 31: 3016.
  55. Herbst RS, Gordon MS, Fine GD, Sosman JA, Soria J-C, Hamid O, et al. A study of MPDL3280A, an engineered PD-L1 antibody in patients with locally advanced or metastatic tumors. *J Clin Oncol.* 2013; 31: 3000.
  56. Natarajan A, Mayer AT, Xu L, Reeves RE, Gano J, Gambhir SS. Novel Radiotracer for ImmunoPET Imaging of PD-1 Checkpoint Expression on Tumor Infiltrating Lymphocytes. *Bioconjug Chem.* 2015; 26: 2062-2069.
  57. England CG, Ehlerding EB, Hernandez R, Rekoske BT, Graves SA, Sun H, et al. Preclinical pharmacokinetics and biodistribution studies of 89Zr-labeled Pembrolizumab. *J Nucl Med.* 2017; 58: 162-8.
  58. Cole EL, Kim J, Donnelly DJ, Smith RA, Cohen D, Lafont V, et al. Radiosynthesis and preclinical PET evaluation of (89)Zr-nivolumab (BMS-936558) in healthy non-human primates. *Bioorg Med Chem.* 2017; 25: 5407-14.
  59. England CG, Jiang D, Ehlerding EB, Rekoske BT, Ellison PA, Hernandez R, et al. 89 Zr-labeled nivolumab for imaging of T-cell infiltration in a humanized murine model of lung cancer. *Eur J Nucl Med Mol Imaging.* 2018; 45: 110-20.
  60. Natarajan A, Patel CB, Habte F, Gambhir SS. Dosimetry prediction for clinical translation of (64)Cu-Pembrolizumab immunoPET targeting human PD-1 expression. *Sci Rep.* 2018; 8: 633.
  61. Natarajan A, Mayer AT, Reeves RE, Nagamine CM, Gambhir SS. Development of novel immunoPET tracers to image human PD-1 checkpoint expression on tumor-infiltrating lymphocytes in a humanized mouse model. *Mol Imaging Biol.* 2017; 19: 903-14.
  62. Du Y, Liang X, Li Y, Sun T, Jin Z, Xue H, et al. Nuclear and fluorescent labeled PD-1-Liposome-DOX-64Cu/IRDye800CW allows improved breast tumor targeted imaging and therapy. *Mol Pharm.* 2017; 14: 3978-86.
  63. Du Y, Sun T, Liang X, Li Y, Jin Z, Xue H, et al. Improved resection and prolonged overall survival with PD-1-IRDye800CW fluorescence probe-guided surgery and PD-1 adjuvant immunotherapy in 4T1 mouse model. *Int J Nanomedicine.* 2017; 12: 8337-51.
  64. Chames P, Van Regenmortel M, Weiss E, Baty D. Therapeutic antibodies: successes, limitations and hopes for the future. *Br J Pharmacol.* 2009; 157: 220-33.
  65. Maute RL, Gordon SR, Mayer AT, McCracken MN, Natarajan A, Ring NG, et al. Engineering high-affinity PD-1 variants for optimized immunotherapy and immuno-PET imaging. *Proc Natl Acad Sci U S A.* 2015; 112: 6506-14.
  66. Mayer AT, Natarajan A, Gordon SR, Maute RL, McCracken MN, Ring AM, et al. Practical immuno-PET radiotracer design considerations for human immune checkpoint imaging. *J Nucl Med.* 2017; 58: 538-46.
  67. Pen JJ, Keersmaecker BD, Heirman C, Corthals J, Liechtenstein T, Escors D, et al. Interference with PD-L1/PD-1 co-stimulation during antigen presentation enhances the multifunctionality of antigen-specific T cells. *Gene Ther.* 2014; 21: 262-71.
  68. Chatterjee S, Lesniak WG, Miller MS, Lisok A, Sikorska E, Wharram B, et al. Corrigendum to "Rapid PD-L1 detection in tumors with PET using a highly specific peptide". *Biochem Biophys Res Commun.* 2017; 491: 1125.
  69. Chatterjee S, Lesniak WG, Miller MS, Lisok A, Sikorska E, Wharram B, et al. Rapid PD-L1 detection in tumors with PET using a highly specific peptide. *Biochem Biophys Res Commun.* 2017; 483: 258-63.
  70. Gonzalez Trotter DE, Meng X, McQuade P, Rubins D, Klimas M, Zeng Z, et al. *In vivo* imaging of the Programmed Death Ligand 1 by (18F) PET. *J Nucl Med.* 2017; 58: 1852-7.
  71. Donnelly DJ, Smith RA, Morin P, Lipovsek D, Gokemeijer J, Cohen D, et al. Synthesis and biological evaluation of a novel (18F)-labeled adnectin as a PET radioligand for imaging PD-L1 expression. *J Nucl Med.* 2018; 59: 529-535.
  72. Dong H, Strome SE, Salomao DR, Tamura H, Hirano F, Flies DB, et al. Tumor-associated B7-H1 promotes T-cell apoptosis: a potential mechanism of immune evasion. *Nat Med.* 2002; 8: 793-800.

73. Patel SP, Kurzrock R. PD-L1 expression as a predictive biomarker in cancer immunotherapy. *Mol Cancer Ther.* 2015; 14: 847-56.
74. Scheerens H, Malong A, Bassett K, Boyd Z, Gupta V, Harris J, et al. Current status of companion and complementary diagnostics: Strategic considerations for development and launch. *Clin Transl Sci.* 2017; 10: 84-92.
75. A. Niemeijer, E. Smit, I. Bahce, O. Hoekstra, M. Huisman, G.A. van Dongen, et al. Whole body PD-1 and PD-L1 PET in pts with NSCLC. *Ann Oncol.* 2017; 28: 460-496.
76. Keyaerts M, Xavier C, Heemskerk J, Devoogdt N, Everaert H, Ackaert C, et al. Phase I study of <sup>68</sup>Ga-HER2-nanobody for PET/CT assessment of HER2 expression in breast carcinoma. *J Nucl Med.* 2016; 57: 27-33.